

Experimental and numerical studies on SCFs of empty SHS-SHS T-joints under in-plane bending

Feleb N Matti, * and Fidelis R Mashiri

School of Computing, Engineering and Mathematics, Western Sydney University, Penrith, Locked bag 1797, NSW 2751, Australia

*Corresponding author's email: f.matti@westernsydney.edu.au

Peer review history

Manuscript submitted: 23 April 2019

Review process completed: 3 August 2019

Manuscript finally accepted: 5 August 2019

Handling Editor: Professor Aatur Rahman

Abstract: This paper presents an experimental and numerical study on square hollow section (SHS) T-joints ($t \leq 4$ mm) subjected to in-plane bending (IPB) on the brace. In the experimental investigation, strain gauges were used to measure the strains and determine the stress concentration factor (SCFs) at the potential hot spot locations (Lines A-E) for each SHS-SHS T-joint specimen. The numerical study was performed by developing three-dimensional finite element models through the use of ABAQUS

software to capture the distribution of the SCF at the weld toes. In this investigation, the empty T-joints are made up of an empty SHS brace and empty SHS chord member. Six empty SHS-SHS T-joints were tested and modelled under static in-plane bending load. The maximum experimental and numerical SCFs will be compared with the SCFs obtained from CIDECT Design Guide 8. There is a good agreement between the numerical results and the experimental results for each identical T-joint connection. This paper provided additional results for smaller β values and larger β values. Results show a similar trend of the variation of SCF with β from experiments and numerical analysis.

Keywords: Stress concentration factor; Empty SHS T-joints; Experimental investigation, Finite element analysis; In-plane bending.

1. Introduction

Thin walled ($t \leq 4$ mm) tubular SHS-SHS T-joints are widely used in truss bridges, high rise buildings, cranes and towers. The T-joint connections in an engineering structure may be subjected to cyclic in-plane bending loads which may cause a structure to collapse. Limited numerical and experimental investigations on unfilled and composite SHS tubular T-joints are available. Feng and Young (2010) conducted a numerical study and design on SHS and rectangular hollow section (RHS) stainless steel tubular T- and X-joints with concrete-filled chords under static compression loading. Tong et al., (2012) tested eight empty circular hollow sections (CHS) to SHS T-connections and developed 3D FE models to determine the SCFs. The CHS-SHS T-connections were tested under axial loading and in-plane bending. In addition, Mashiri et al., (2004) carried out fatigue tests on T-connections made up of CHS brace to SHS chord. Mashiri et al., (2004) measured stress distributions at hot spot locations, where cracks initiated and propagated resulting fatigue failure. Feng et al., (2017) carried out a numerical and experimental static behaviour investigation on both collar plate and doubler plate reinforced SHS T-joints. Eleven SHS T-joints were tested under axial compression. In their investigation, they concluded that large value of β ratio benefits the initial stiffness and the joint strength but deteriorates the ductility.

Mashiri and Zhao (2010) tested empty and concrete-filled SHS-SHS steel tubular T-joints under in-plane bending. Matti and Mashiri (2018) used ABAQUS software to model identical T-joints used in Mashiri and Zhao (2010) experimental investigation to obtain SCFs and compare the SCF determined from the numerical study with the experimental study. The non-dimensional parameter (β) range of the specimens used in Mashiri and Zhao (2010) investigation is $0.35 \leq \beta \leq 0.67$. Therefore, in this paper, more SCF investigations of SHS T-joints was carried out in order to provide more information on the behavior of SHS T-joint specimens. This is achieved by testing SHS T-joints with larger β values ($\beta > 0.67$) and smaller β values ($\beta < 0.35$). There is a good agreement between the numerical SCFs and the experimental SCFs. The experimental and numerical results show a similar trend of the variation of SCF with β .

2. Methodology

2.1 Test series and materials

Six empty SHS-SHS T-joints were tested experimentally and numerically. Table 1 lists the six empty T-joint connections with their dimensions and non-dimensional parameters. The SHS T-joints have non-dimensional parameters, β ranging from 0.25 to 1, 2γ ranging from 25 to 33.33 and τ ranging from 0.75 to 1.0. As shown in Table 1, the steel SHSs used in this investigation are cold-formed and have a steel grade of C350LO which comply with AS1163-2009 (Standards Australia Online 2009). The external corner radii of the empty tubes were calculated according to OneSteel Market Mills (2004). The corner radii were determined based on the size and thickness of the sections. The design tensile strength of the steel is 430 MPa, in accordance to AS 4100-1998 (Standards Australia Online 1998). The SHS chord of each T-joint connection is welded to an SHS brace at right angles. The size of the weld defined by the leg length and throat thickness was determined in accordance to AS 4100-1998 (Standards Australia Online 1998) which equal to 6 mm and 4.24 mm, respectively. According to AS 4100-1998 (Standards Australia Online 1998), the nominal tensile strength of the weld metal is 480 MPa.

Table 1. Connection series used in this numerical investigation to determine the SCFs.

Series	Chord $d_o \times b_o \times t_o$ mm \times mm \times mm	Brace size $d_1 \times b_1 \times t_1$ mm \times mm \times mm	Non-dimensional parameters			Steel grade	Length	
			$\beta = \frac{b_1}{b_o}$	$2\gamma = \frac{b_o}{t_o}$	$\tau = \frac{t_1}{t_o}$		Brace (mm)	Chord (mm)
S6S1	100×100×4 SHS	25×25×3 SHS	0.25	25	0.75	C350LO	500	600
S5S1	100×100×3 SHS	25×25×3 SHS	0.25	33.33	1.00		500	600
S6S2	100×100×4 SHS	40×40×3 SHS	0.40	25	0.75		500	600
S6S3	100×100×4 SHS	50×50×3 SHS	0.50	25	0.75		500	600
S6S4	100×100×4 SHS	75×75×3 SHS	0.75	25	0.75		500	600
S5S5	100×100×3 SHS	100×100×3 SHS	1.00	33.33	1.00		500	600

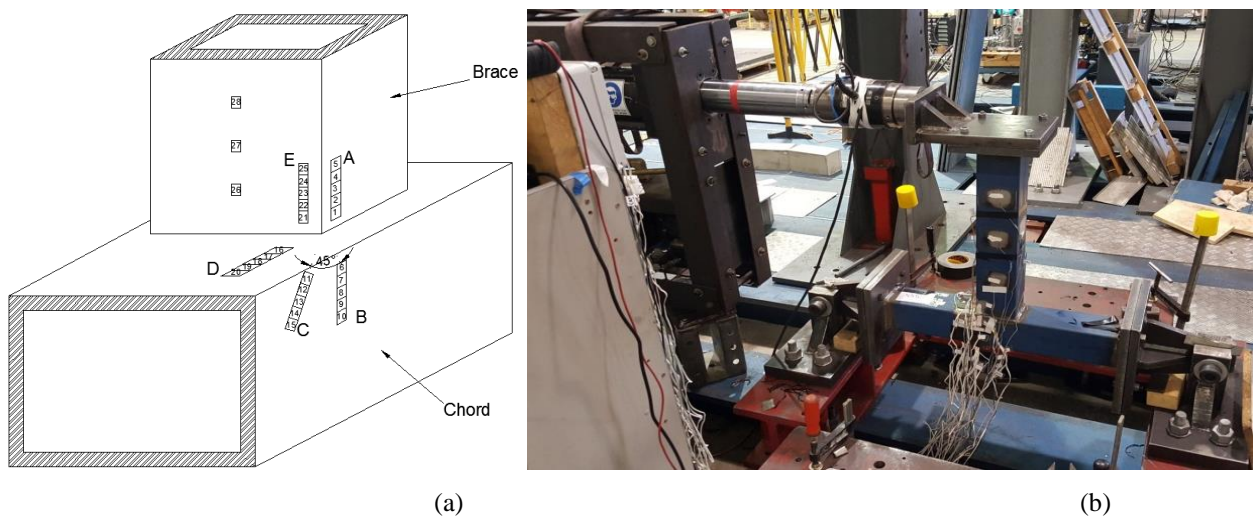


Figure 1. Locations of strain gauges: (a) Schematic diagram; and (b) Test rig: in-plane bending.

2.2 Instrumentation and test setup

Single and strip strain gauges were attached onto six empty SHS T-joint specimens to measure the strains. The locations of the single and strip strain gauges are shown in Figure 1(a). Each specimen consisted of 3 single strain gauges and 5 strip strain gauges. The strip strain gauges comprise of 5-element single strain gauges. The gauges in a strip strain gauge are at 2 mm apart. The strain gauges were installed using Cyanoacrylate Strain Gauge Glue. As shown in Figure 1(a), strip strain gauges were installed along the chord and brace intersections at lines A, B, C, D and E. As recommended by Zhao et al., (2001), the distance of the strain gauge from the weld toe is the lesser of $0.4t$ or 4 mm but a minimum of 4 mm. For this investigation, the first strain gauge of the strip strain gauge closest to the weld toe was installed at 4 mm from the weld toe as all tubes had a thickness less than 10 mm.

The T-joint specimens were connected to the test rig through M12 bolts of grade 8.8 snug tight. The testing of the specimens was setup under in-plane bending loads on the brace. The test setup displayed in Figure 1(b) was used to measure the strain distribution. In-plane bending moment loads were applied to each specimen. In-plane bending means that the load is being applied to the brace in the direction of the longitudinal axis of the chord. In order to carry out high-cycle fatigue tests or determine SCFs, the loads that are applied to each T-joint specimen are within the elastic response range of the load-deformation curve of the SHS-SHS T-joint. Each specimen consisted of two end plates which were bolted to the end brackets to support the T-joint connection.

2.3 Finite element modelling (FEM)

The finite element method (FEM) is a great method in determining the SCFs of a connection. Linear elastic FEA modelling was carried out to determine the SCFs at the location of interest at which the SCFs were experimentally determined, line A to E. Six empty SHS-SHS T-joints were modelled and tested under static in-plane bending load on the brace using ABAQUS software. The non-dimensional parameters of the empty T-joints specimens are the same as the T-joint models. Since there is no buckling in the T-joint and the load is within the elastic response region, geometric imperfections were not included in the finite element modelling. The pinned supports can resist vertical and horizontal forces but not a moment which will allow the T-joint specimens to rotate about the x-direction. The weld was tied to the end plates and the chord ends as well as the top plate and the top end of the brace. Furthermore, the weld was tied with the brace and chord intersection.

The finite element type that has been used for the models is 8 noded ABAQUS C3D8R 3D linear hexahedral solid elements. A static horizontal in-plane bending load was applied in the middle of the T-joints' top plate as shown in Figure 2 using the Static, General procedure available in the ABAQUS library. The SHS-SHS T-joint models were subjected to in-plane bending load on the brace. The load that is applied to each concrete-filled SHS-SHS T-joint specimens is within the elastic response range of the load-deformation curve of the SHS-SHS T-joint. Since tension is more critical for fatigue, crack opening and crack growth, the stress values at lines A, B, C, D and E will be obtained on the side under tension. The hot spot locations to measure the stresses are shown in Figure 2. As shown in Figure 2, each line comprises of 5 nodes representing the number of strain gauges in a strip strain gauge since each strip gauge consist of five strain gauges. The mesh for the welded T-joints was generated on parts that were created within ABAQUS. Whole models were meshed and included in the simulation. Figure 2 shows a typical meshed model with different mesh densities to meet the needs of this analysis. Feleb and Mashiri (2018) conducted a mesh sensitivity analysis to find the optimum mesh for these connections. Finer element edge, 1 mm in length was used at lines A-E.

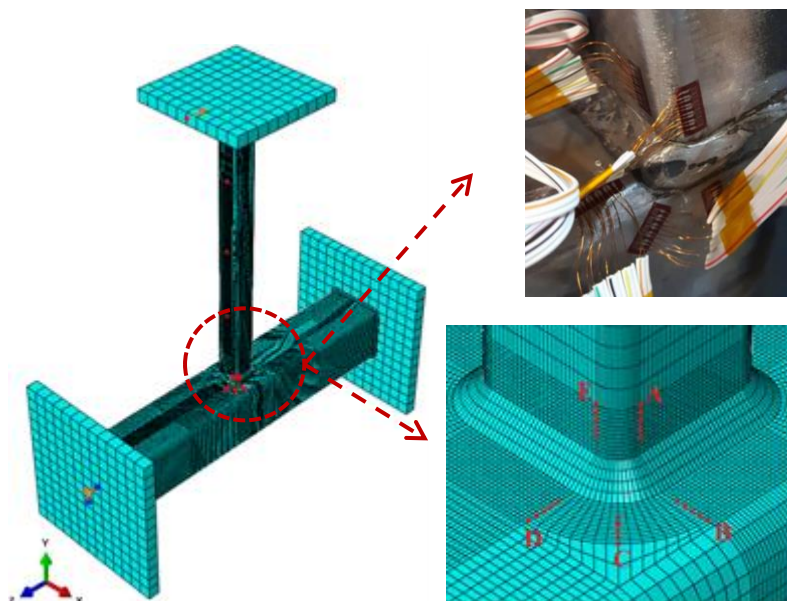


Figure 2. FE mesh model with hot spot locations.

3. Stress concentration factors (SCFs)

3.1 Experimental SCF

The SCF_{SHS} at a hot spot location in the square hollow section T-joints was calculated using equation 1 as recommended by Zhao et al., (2001). The $SNCF_{SHS}$ for each load case was calculated using equation 2.

$$SCF_{SHS, Experimental, A-E} = 1.1 \times SNCF_{SHS} \tag{1}$$

$$SNCF_{SHS} = \frac{\text{Hot Spot Strain (HSSN)}}{\text{Nominal Strain}} \tag{2}$$

The hot spot strain for each load case was calculated through the use of quadratic extrapolation. Figure 3 compares the two extrapolation methods; linear and quadratic extrapolation in determining the hot spot strains for a typical T-joint specimen along line A. Figure 3 shows that the quadratic hot spot strains are higher than the linear hot spot strains. In rectangular hollow sections (or SHS), Zhao et al., (2001) recommended the use of the quadratic extrapolation method as the distribution of the stresses is non-linear. Mashiri and Zhao (2010) used quadratic extrapolation for the determination of the hot spot stresses. Quadratic extrapolation was therefore adopted in this investigation for lines A to E.

The values of the nominal strain values for in-plane bending were calculated by the linear extrapolation method using the extrapolation points on the tension side of the brace, see Figure 2. Since strains were measured at four (4) load levels, four (4) SNCFs values were calculated for each strip strain gauge and for each location from line A to E. The average value of the SNCFs is the strain concentration factor for the connection ($SNCF_{SHS}$) for each strip strain gauge.

3.2 Numerical SCF

Mashiri (2001) defined the stress concentration factor to be the ratio of the hot spot stress (σ_{hss}) and the nominal stress (σ_{nom}) for a member in a chord-brace connection subjected to in-plane bending load on a brace member. Equation 3 expresses the numerical SCF for each hot spot location (line A-E).

$$SCF_{SHS, Numerical, A-E} = \frac{\text{hot spot stress } (\sigma_{hss})}{\text{nominal stress } (\sigma_{nom})} \tag{3}$$

The hot spot stress for each hot spot location (line A-E) was calculated through the use of quadratic extrapolation. Figure 4 compares linear and quadratic extrapolation in determining the hot spot stress at the weld toe for a typical T-joint specimen. The hot spot stresses occur at the weld toe. Furthermore, Figure 4 shows that the quadratic hot spot stresses are higher than the linear hot spot stresses. Numerical nominal stresses were calculated using the linear extrapolation method, as shown in Figure 5(a). For comparison, beam theory nominal stresses were also calculated using the ratio of the bending moment (M) in the brace and the elastic section modulus of the brace (Z). This method is known as the simple beam theory which expresses nominal stress as follows: $\sigma_{nom} = M/Z$. As illustrated in Table 2 and Figure 5(b), the value of the numerical nominal stress (FEA) for each SHS T-joint is similar to the beam theory nominal stress.

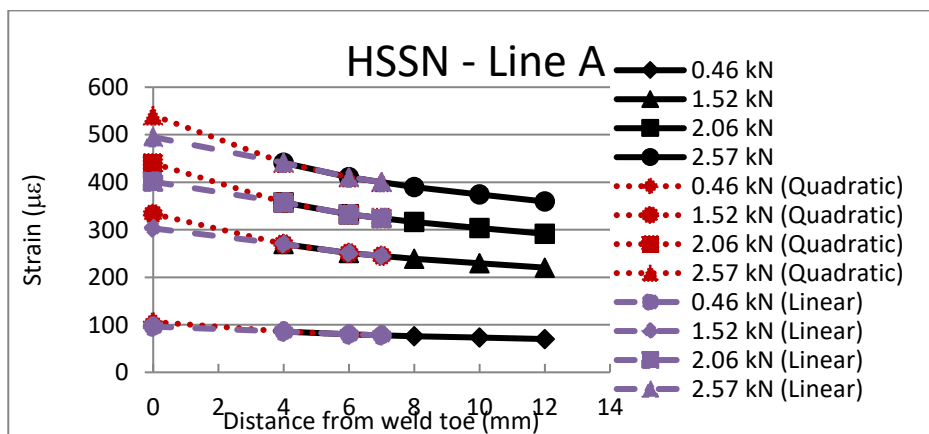


Figure 3. Determination of hot spot strain (HSSN)

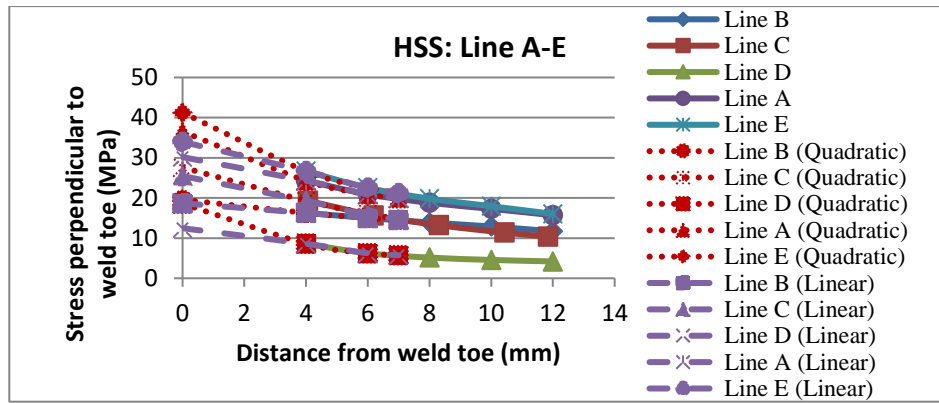


Figure 4. Determination of hot spot stress (σ_{hss}).

In finite element modelling, the typical stress distribution of an SHS-SHS T-joint specimen is shown in Figure 6(a) and (b). This figure shows that the SHS T-joint specimens with lower non-dimensional parameter, β have greater stresses than the SHS T-joint specimen with higher β if subjected to same loading.

Table 2. Nominal stresses.

Model	$D_{B.MID}$ (mm)	$\sigma_{B.MID}$ (MPa)	$D_{B.QTR}$ (mm)	$\sigma_{B.QTR}$ (MPa)	$D_{B.END}$ (mm)	$\sigma_{nom.num}$ Numerical (MPa)	$\sigma_{nom.exp}$ Beam Theory (MPa)	Ratio $\frac{\sigma_{nom.exp}}{\sigma_{nom.num}}$
S6S1	250	99.39	375	51.27	0	195.62	208.16	1.06
S5S1	250	99.39	375	51.27	0	195.62	208.16	1.06
S6S2	250	32.10	375	16.56	0	63.19	65.67	1.04
S6S3	250	19.36	375	9.99	0	38.11	39.28	1.03
S6S4	250	7.97	375	4.11	0	15.70	16.02	1.02
S5S5	250	4.32	375	2.23	0	8.51	8.64	1.01
Average								1.04

Note: $D_{B.MID}$ = distance.brace.middle; $\sigma_{B.MID}$ = stress.brace.middle; $D_{B.QTR}$ = distance.brace.quarter; $\sigma_{B.QTR}$ = stress.brace.quarter; $D_{B.END}$ = distance.brace.end; $\sigma_{nom.exp}$ = experimental nominal stress; $\sigma_{nom.num}$ = numerical nominal stress.

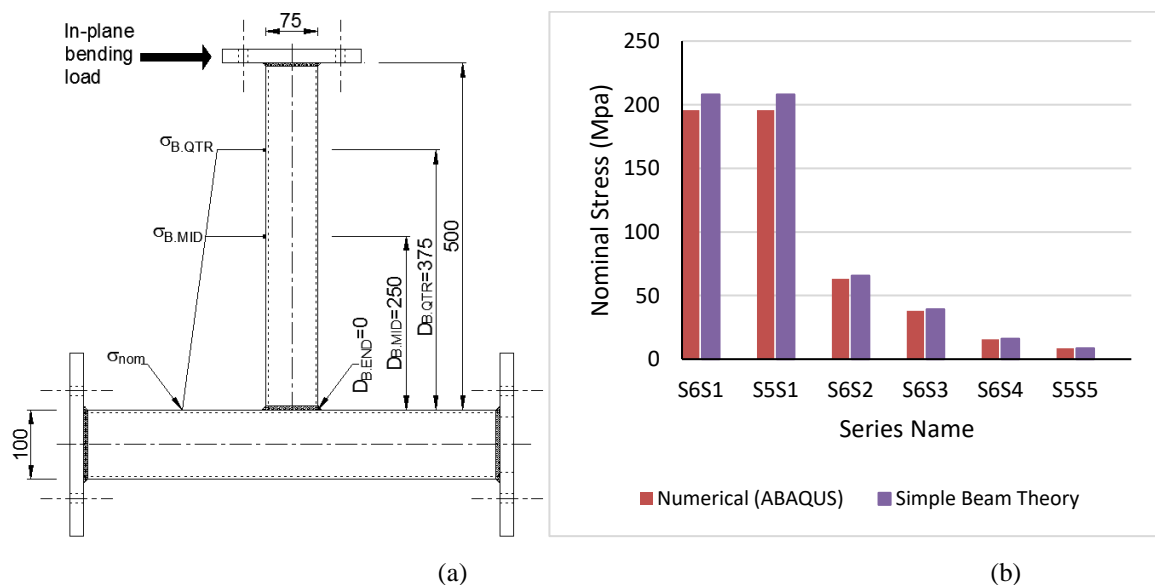


Figure 5. Nominal stresses: (a) extrapolation points; and (b) numerical and beam theory results.

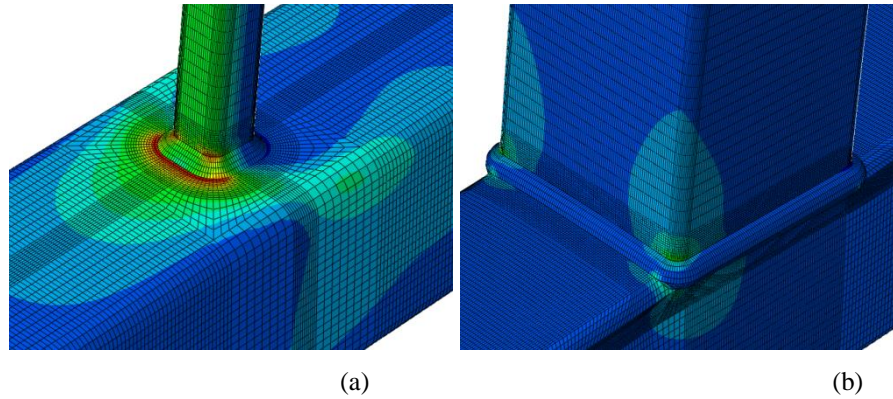


Figure 6. Stress distribution of empty T-joints subjected to IPB: (a) Empty S6S1; and (b) Empty S5S5.

3.3 SCF using CIDECT Design Guide

The SCFs for hollow SHS-SHS T-joint under in-plane bending on the brace were calculated through the use of CIDECT Design Guide 8 (Zhao et al., 2001). The SCFs obtained from the Design Guide (empty SHS-SHS T-joints) will be compared with the SCFs determined from the experimental and numerical studies. Comparing the SCFs results between the Design Guide with experiment and the finite element models, will enable the validation of the results. Equations 4-7 were used to determine the SCFs of empty SHS-SHS T-joints under in-plane bending along lines A to E:

$$SCF_{B,ipb} = (-0.011 + 0.085 \times \beta - 0.073 \times \beta^2) \times (2\gamma)^{(1.722+1.151 \times \beta - 0.697 \times \beta^2)} \times \tau^{0.75} \quad (4)$$

$$SCF_{C,ipb} = (0.952 - 3.062 \times \beta + 2.382 \times \beta^2 + 0.0228 \times 2\gamma) \times (2\gamma)^{(-0.690+5.817 \times \beta - 4.685 \times \beta^2)} \times \tau^{0.75} \quad (5)$$

$$SCF_{D,ipb} = (-0.054 + 0.332 \times \beta - 0.258 \times \beta^2) \times (2\gamma)^{(2.084-1.062 \times \beta + 0.527 \times \beta^2)} \times \tau^{0.75} \quad (6)$$

$$SCF_{A,ipb} = SCF_{E,ipb} = 1.4 \times (0.390 - 1.054 \times \beta + 1.115 \times \beta^2) \times (2\gamma)^{(-0.154+4.555 \times \beta - 3.809 \times \beta^2)} \quad (7)$$

4. Results and discussion

4.1. SCFs

Table 3 and Figure 7 show the distribution of the SCF and the maximum SCFs in the six empty SHS-SHS T-joints. The ratios of the maximum SCF in FEA model to that in experiment; $(SCF_{ABAQUS}/SCF_{Experiment})$ are given in Table 3. These ratios are close to 1 and the average ratio is 1.04. Therefore, it can be stated that a good agreement is achieved between the numerical SCF results and the experimental SCF results for each identical T-joint connection.

On the other hand, the average ratio of the maximum empty SCF in FEA model to that in CIDECT Design guide; $(SCF_{ABAQUS}/SCF_{CIDECT})$ is 0.58, given in Table 3. The SCFs of the CIDECT Design Guide are higher than both the experimental and the numerical SCFs. This is beneficial for fatigue design assessments as a conservative estimate of life is given by higher SCF. Figure 7 shows that for the majority of the SCF results, similar trends can be seen between CIDECT, Experimental and numerical SCFs. The maximum SCFs on the FE models in S6S1, S5S1, S6S2, S6S3, S6S4 and S5S5 occurred along line C, D, C, C, B and E, respectively. The maximum experimental SCFs in S6S1, S5S1, S6S2, S6S3, S6S4 and S5S5 occurred along line D, C, D, D, A and A, respectively. Similarly, the maximum SCFs based on the CIDECT Design Guide in S6S1, S5S1, S6S2, S6S3, S6S4 and S5S5 occurred along line D, D, C, C, C and A (and E), respectively.

In summary, the majority of the maximum SCFs occurred at line C and D excluding S5S5 where the maximum experimental, numerical and CIDECT SCFs occurred on the brace at line A and/ or E. The non-dimensional parameter (β) of S5S5 T-joint connection is 1.

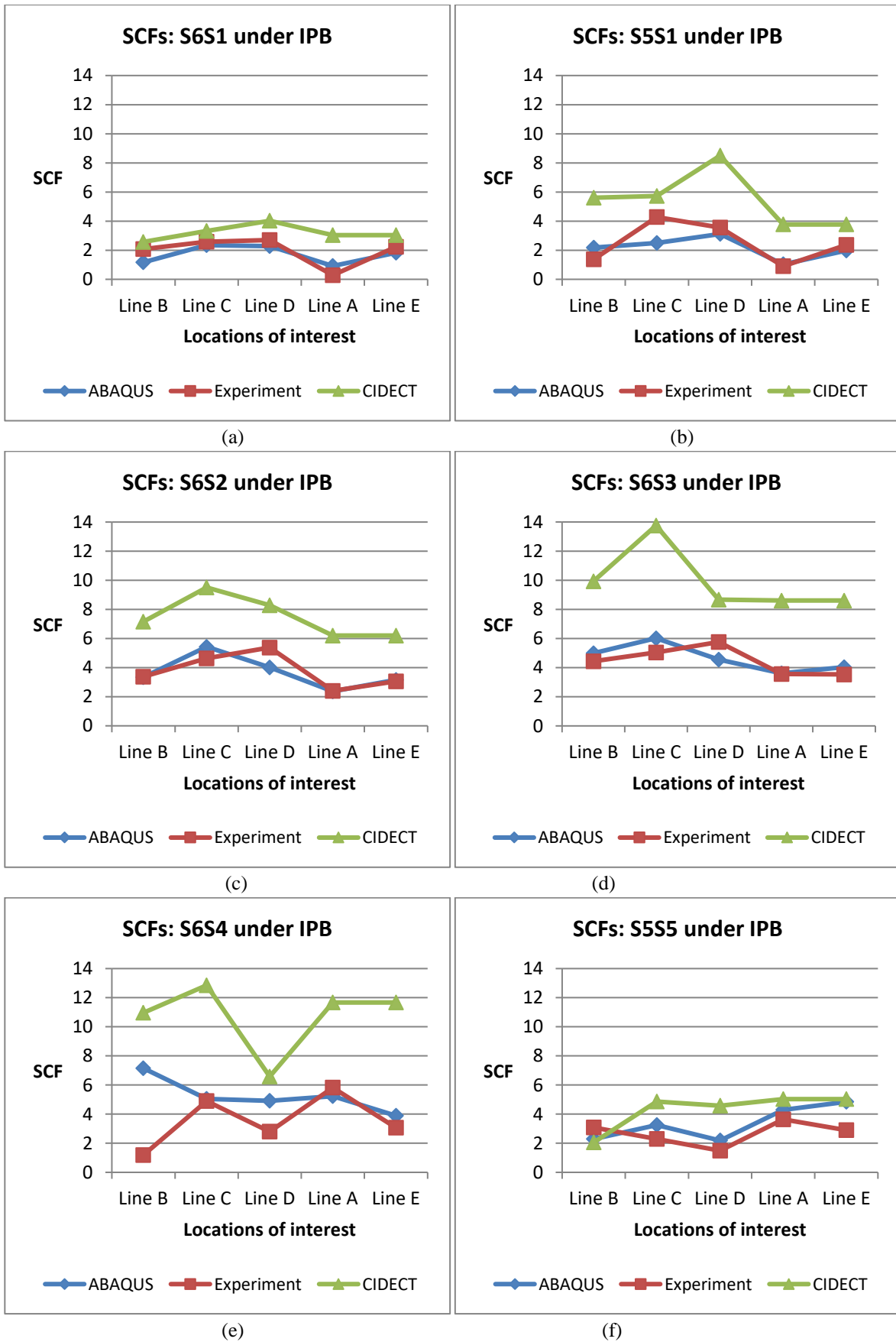


Figure 7. Comparison of SCFs in empty SHS-SHS T-joints under in-plane bending: (a) Empty S6S1; (b) Empty S5S1; (c) Empty S6S2; (d) Empty S6S3; (e) Empty S6S4; and (f) Empty S5S5.

Table 3. SCFs in unfilled T-joints under in-plane bending.

Series name	ABAQUS/ Experiment/ CIDECT	SCF (quadratic) Empty SHS T-joints					Ratio of maximum SCFs	
		B	C	D	A	E	$\frac{SCF_{ABAQUS}}{SCF_{Experiment}}$	$\frac{SCF_{ABAQUS}}{SCF_{CIDECT}}$
S6S1	ABAQUS	1.16	2.35	2.28	0.92	1.82	0.87	0.58
	Experiment	2.07	2.58	2.70	0.28	2.22		
	CIDECT	2.57	3.33	4.02	3.04	3.04		
S5S1	ABAQUS	2.18	2.50	3.11	1.03	1.98	0.73	0.37
	Experiment	1.37	4.27	3.55	0.90	2.37		
	CIDECT	5.61	5.72	8.50	3.77	3.77		
S6S2	ABAQUS	3.34	5.43	4.02	2.37	3.17	1.00	0.57
	Experiment	3.38	4.65	5.38	2.41	3.06		
	CIDECT	7.16	9.51	8.28	6.20	6.20		
S6S3	ABAQUS	5.00	6.02	4.55	3.61	4.03	1.05	0.44
	Experiment	4.45	5.04	5.76	3.57	3.54		
	CIDECT	9.92	13.76	8.67	8.61	8.61		
S6S4	ABAQUS	7.15	5.06	4.92	5.24	3.89	1.23	0.56
	Experiment	1.19	4.90	2.80	5.82	3.07		
	CIDECT	10.96	12.85	6.58	11.66	11.66		
S5S5	ABAQUS	2.30	3.24	2.19	4.29	4.85	1.33	0.96
	Experiment	3.08	2.29	1.49	3.64	2.90		
	CIDECT	2.06	4.86	4.57	5.03	5.03		
Average							1.04	0.58

4.2. The influence of β

The geometric parameters' influence on fatigue strength and SCFs under in-plane bending was investigated. The chord width (b_0) of each specimen is the same. Therefore, it can be stated that the change in brace width (b_1) of each SHS-SHS T-joint connection influences the non-dimension parameter (β), see Table 1. Since the non-dimensional parameter (β) of the specimens is not the same, different SCFs were obtained under in-plane bending. Figure 8 shows the maximum SCF against the non-dimensional parameter, β for empty SHS-SHS T-joints under in-plane bending. As shown in Figure 8 (a), the values of the maximum experimental and numerical SCFs of SHS T-joints with $2\gamma=25$ and $\tau=0.75$ increase with the increased value of β . The maximum SCF using CIDECT Design Guide also increases with the increased value of β but slightly decreased when $\beta=0.75$. Furthermore, as shown in Figure 8 (b), the values of the numerical and CIDECT SCFs of SHS T-joints with $2\gamma=33.33$ and $\tau=1$ increase with the increased value of β and decreased when β equals to 1. It should be noted that the two experimental SCFs at $\beta = 0.35$ and 0.5 shown in Figure 8 (b) were obtained from Mashiri and Zhao (2010) since these two T-joint specimens were not tested in this experimental study. Figure 8 (b) shows that the maximum experimental SCF reduced when $\beta = 0.5$ and continued reducing when $\beta = 1$. In summary, similar trends can be observed between CIDECT, Experiment and numerical peak SCFs.

4.3. Failure mode

As shown in Figure 9, for empty T-joint under in-plane bending, the chord face deformation is in both tensile and compressive region. Similar failure mode between CIDECT Design Guide 3 (Packer et al., 2009) and the FE model was achieved.

5. Conclusion

An experimental and a numerical study on unfilled square hollow section (SHS) T-joints under static in-plane bending were carried out. For the experimental investigation, strain gauges were installed onto six empty SHS T-joints to determine the stress concentration factor (SCF) at the hot spot locations (Lines A-E). The numerical study was carried out by developing 3D T-joint models identical to the experimental T-joint specimens using ABAQUS software to capture the distribution of the SCF. SCFs under in-plane bending using CIDECT Design Guide 8 (Zhao et al., 2001) were also obtained and compared with the experimental and numerical SCFs.

A good agreement is achieved between the numerical results and the experimental results for each identical non-dimensional parameter T-joint. The ratios of the maximum empty SCF in FEA model to that in experiment; ($SCF_{ABAQUS}/SCF_{Experiment}$) are close to 1 and the average ratio is 1.04. The average ratio of the maximum empty SCF in

FEA model to that in CIDECT Design guide; ($SCF_{ABAQUS}/SCF_{CIDECT}$) is 0.58. The SCFs of the CIDECT Design Guide are higher than both the experimental and the numerical SCFs. This is beneficial for fatigue design assessments as a conservative estimate of life is given by higher SCF.

The majority of the maximum SCFs occurred at line C and D excluding S5S5 where the maximum experimental, numerical and CIDECT SCFs occurred on the brace at line A and/ or E. Furthermore, the failure mode of the welded empty tubular T-joints under in-plane bending between CIDECT Design Guide 3 (Packer et al., 2009) and the FE model are the same. For empty T-joints, the chord face deformations are in both tensile and compressive regions.

The non-dimension parameter (β) influences on fatigue strength and SCFs under in-plane bending. Since the non-dimensional parameter (β) of the specimens is not the same, different SCFs were obtained under in-plane bending. The values of the maximum experimental and numerical SCFs increase with the increased value of β . The maximum SCF using CIDECT Design Guide also increases with the increased value of β but slightly decreased when $\beta=0.75$. The numerical and CIDECT SCFs increase with the increased value of β and decreased when β equals to 1. The maximum experimental SCF reduced when $\beta = 0.5$ and continued reducing when $\beta = 1$.

In the future, experimental, numerical and parametric studies on empty SHS T-joints under axial loads and out-of-plane bending on the brace will be explored. Furthermore, experimental, numerical and parametric studies on SHS T-joints with concrete-filled chord will be investigated under axial loadings, in-plane bending and out-of-plane bending.

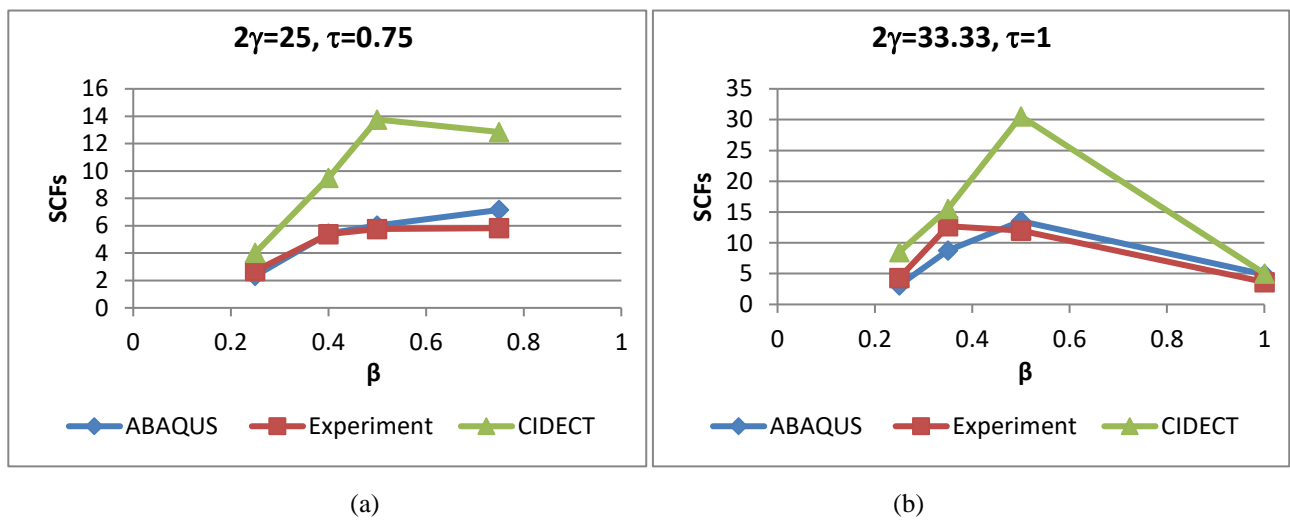


Figure 8. Variations of maximum SCFs with β under IPB: (a) $2\gamma=25, \tau=0.75$; and (b) $2\gamma=33.33, \tau=1$.

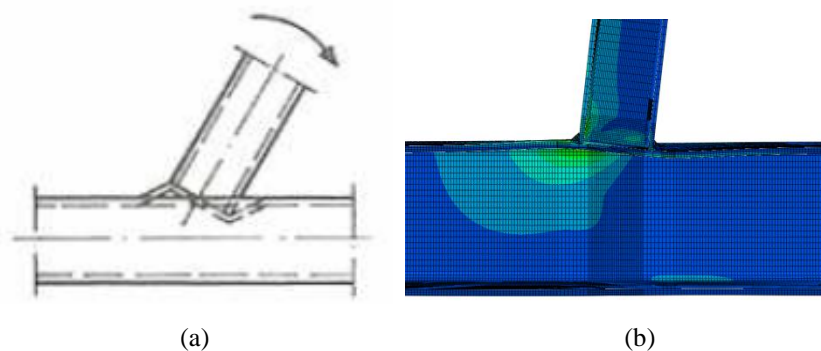


Figure 9. Failure mode under IPB: (a) Empty (Packer et al., 2009); and (b) Typical empty (FE model).

6. Acknowledgements

The authors are thankful to Western Sydney University (WSU) for funding sources and supporting this project. The authors wish to thank the WSU laboratory staff; Mr. Murray Bolden and Mr. Robert Marshall for their assistance in performing the experimental test in the lab.

7. References

- Zhao, X. L., Herion, S., Packer, J. A., Puthli, R. S., Sedlacek, G., Wardenier, J., Weynand, K., van Wingerde, A. M., & Yeomans, N. F. (2001). Design guide for circular and rectangular hollow section welded joints under fatigue loading. TÜV-Verlag.
- Feng, R., & Young, B. (2010). Design of concrete-filled stainless steel tubular connections, *Advances in Structural Engineering*, 13(3), 471-92.
- Tong, L.W., Zheng, H.Z., Mashiri, F. R., & Zhao, X. L. (2012). Stress-concentration factors in circular hollow section and square hollow section T-connections: experiments, finite-element analysis, and formulas. *Journal of Structural Engineering*, 139(11), 1866-81.
- Mashiri, F. R., Zhao, X. L., & Grundy, P. (2004). Stress concentration factors and fatigue behaviour of welded thin-walled CHS-SHS T-joints under in-plane bending. *Engineering Structures*, 26(13), 1861-75.
- Feng, R., Chen, Y., & Chen, D. (2017). Experimental and numerical investigations on collar plate and doubler plate reinforced SHS T-joints under axial compression. *Thin-Walled Structures*, 110, 75-87.
- Mashiri, F. R., & Zhao, X. L. (2010). Square hollow section (SHS) T-joints with concrete-filled chords subjected to in-plane fatigue loading in the brace. *Thin-Walled Structures*, 48(2), 150-8.
- Matti, F.N., & Mashiri, F. R. (2018). Numerical study on SCFs of empty and concrete-filled SHS-SHS T-joints under in-plane bending. In *Proceedings of the 9th International Conference on Advances in Steel Structures* (P. 875-886). China.
- Standards Australia Online. (2009). Cold-formed structural steel hollow sections. AS 1163-2009, viewed 24 July 2017, SAI Global database.
- OneSteel Market Mills. (2004). Cold formed structural hollow sections & profiles. 4th edn.
- Standards Australia Online. (1998). Steel structures. AS 4100-1998 viewed 27 November 2017, SAI Global database.
- Mashiri, F. (2001). Thin-walled tubular connections under fatigue loading. Doctor of Philosophy thesis, Monash University.
- Packer, J. A., Wardenier, J., Zhao, X. L., van der vegte, G. J., & Kurobane, Y. (2009). Design guide for rectangular hollow section (RHS) joints under predominantly static loading. 2nd edn, Verlag TÜV Rheinland.